**Ali D. Boloorani**
Department of RS&GIS, Faculty of Geography, University of Tehran, Tehran, Iran. Corresponding Author, Email: ali.darvishi@ut.ac.ir

**Masoud Soleimani**
Department of RS&GIS, Faculty of Geography, University of Tehran, Tehran, Iran.
masoud.soleimani@ut.ac.ir

**Ramin Papi**
Department of RS&GIS, Faculty of Geography, University of Tehran, Tehran, Iran.
raminpapi@ut.ac.ir

**Seyed K. Alavipanah**
Department of RS&GIS, Faculty of Geography, University of Tehran, Tehran, Iran. salavipa@ut.ac.ir

**Ayad M. F. Al-Quraishi**
Environmental Engineering Department, College of Engineering, Knowledge University, Erbil, Kurdistan Region, Iraq
ayad.alquraishi@gmail.com

Received on: 19/05/2019
Accepted on: 17/04/2019
Published online on: 25/07/2019

# Zoning Areas Susceptible to Land Subsidence in Tigris and Euphrates Basins

***Abstract***-*Land Subsidence is considered as one of the riskiest hazards in nature and geology. It may be caused by human activities including but not limited to long-term depletion of water, petroleum, and gas from underground reservoirs. Monitoring and zoning of regions susceptible to land-subsidence within Tigris and Euphrates rivers basin can play a major role in predicting and preventing damages from subsidence and can aid in better planning for utilizing its water resources. Accordingly, this study proposed to employ 9 effective parameters on subsidence including: precipitation, total water underground changes, elevation, slope, population, land use, distance from petroleum and gas fields, distance from faults, and distance from rivers. Decision Making Trial and Evaluation Laboratory method was applied for analyzing relationships between parameters. Fuzzy Analytical Hierarchy Process and Boolean methods were combined to produce zoning maps of Tigris and Euphrates basin subsidence. The results were indicative of the high potential of subsidence in zones contributing to 1.39% of the total area of the Tigris and Euphrates basin. Inter-parameter analysis by using of Decision Making Trial and Evaluation Laboratory indicated that land cover, total water underground changes, and population were the most impressible factors in land subsidence zoning, respectively.*

***Keywords***- *Land subsidence zoning, Remote Sensing, Tigris and Euphrates Basin*

**How to cite this article:** A.D. Boloorani, M. Soleimani, R. Papi, S.K. Alavipanah and A.M.F. Al-Quraishi, "Zoning Areas Susceptible to Land Subsidence in the Tigris and Euphrates Basin," *Engineering and Technology Journal*, Vol. 37, Part A, No. 7, pp. 265-272, 2019.

## 1. Introduction

Land subsidence is defined as the gradual or sudden settling of ground surface due to the condensation of subterranean materials. One of its most common causes is the irregular discharge of aquifers. In fact, numerous studies have confirmed the occurrence of subsidence due to aquifer discharge [1, 2, 3, 4, 5, 6]. Subsidence may occur as the result of condensation of subterranean materials when groundwater discharge is carried out at a rate faster than its recharge [7]. Decreases rainfall and successive droughts during the past few decades have caused a shortage in surface water supply and have further prevented natural groundwater recharge. The expanding growth of urban populations and the resulting increase in water demands (urban, industrial, and agricultural) have led to the excessive discharge and depletion of groundwater as well as subsidence. These circumstances are in fact a warning of a greater global crisis, which may bring about serious environmental consequences including damages to man-built structures, roads, bridges, power transmission lines, incisions on the ground's surface, and flood [8,9].

http://dx.doi.org/10.30684/etj.37.7A.7
2412-0758/University of Technology-Iraq, Baghdad, Iraq

## 2. Methodology

Figure 1 shows a flowchart of the overall schema of this study. As can be seen, following the identification of the effective factors on subsidence, raw data (Table 1) are collected and preprocessed for each parameter (Figure 2). The processed data are then used to produce zoning maps of subsidence using Fuzzy Analytical Hierarchy Process (FAHP) and Boolean methods. These two methods are then combined to give the final zoning map, and relationships between the parameters were analyzed using Decision Making Trial and Evaluation Laboratory (DEMATEL) method.

Data from the Gravity Recovery and Climate Experiment (GRACE) satellite were used for the temporal monitoring of total water underground changes (TWUC). Accordingly, spherical harmonic coefficients from the GFZ (version 05) processing center from April 18, 2002 to January 21, 2017 were used. A total of 159 monthly products were ultimately processed for measuring changes in total water storage (TWS) or rather monthly Equivalent Water Height (EWH). The data were processed using the proposed method by [10, 11] as so:

$$EWH(\varphi,\lambda) = {}^{a\rho_{ave}}/_{3\rho_w} \sum_{l=0}^{\infty} \sum_{m=0}^{l} {}^{2l+1}/_{1+K_l} \tilde{p}_{lm}(\sin\varphi)[\Delta C_{lm}\cos(m\lambda) + \Delta S_{lm}\sin(m\lambda)] \quad (1)$$

Where, EWH shows changes in equivalent water height (cm), φ is the longitude, λ is latitude, α is earth's radius ($6380\,Km$), $\rho_{ave}$ shows earth's average density ($5517\ Kg/m^3$), $\rho_w$ is the density for water ($\sim 1000\ Kg/m^3$), $K_l$ is the love number of degree I, $\tilde{p}_{lm}$ shows normalized Legendre functions, and $\Delta C_{lm}$ and $\Delta S_{lm}$ are the monthly changes in spherical harmonics of degree I and order m. $C_{20}$ (of degree 2 and order 0) was obtained based on the method proposed by [12] using a spherical harmonic degree 2 estimated from the Satellite Laser Ranging (SLR). The first degree spherical harmonic (Geo-center) was also obtained using the method by [13]. Effects of Glacial Isostatic Adjustment (GIA) on the total area of study were negligible. A Gaussian filter (300 Km radius) was also applied to decrease the effects of noisy data [14]. After eliminating the hydraulic effects of the GLDAS model consist of changes in soil moisture, snow water equivalent, and surface water (Table 2), GRACE data were used to obtain monthly changes in groundwater from 2002 to 2017 according to equation 2 [15]. TWUC maps were finally obtained (Figure 2.b).

$$G = S - SWE - SW - SM \quad (2)$$

Where, G shows changes in groundwater, S shows changes in TWS (GRACE data), SWE is the snow water equivalent changes, SW shows changes in surface water (rivers and canopy water storage), and SM is changes in soil moisture.

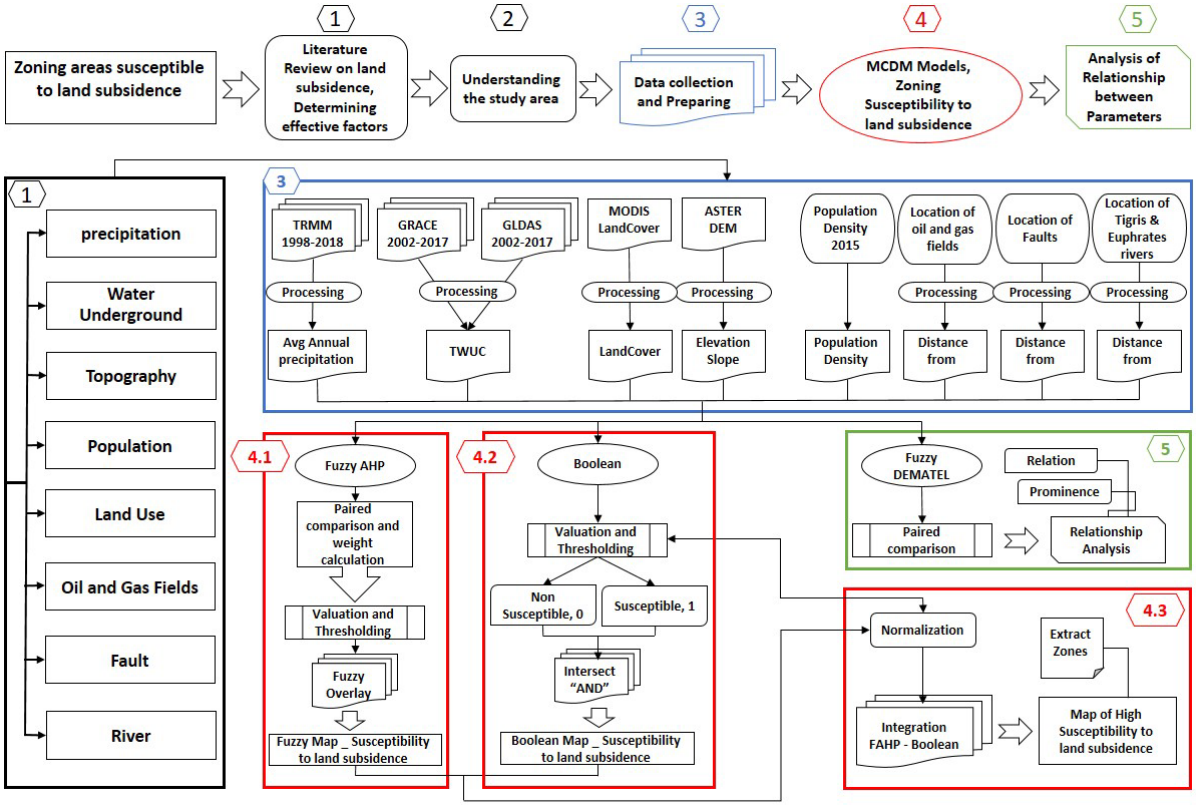


**Figure 1. Zoning areas susceptible to land subsidence in Tigris and Euphrates Basin_ an overview of the methodology**

**Table 1: Data Description**

| Data | Format Type | Resolution ($km^2$) | Time Period | Target Parameter |
|---|---|---|---|---|
| TRMM_Rainfall | GRID (NetCDF4) | ≅25 | 1998-2018 | Average Annual Cumulative Precipitation 1998-2018 |
| GRACE_GFZ | txt (.gz) | ≅111 | 2002-2017 | Total Water Underground Changes 2002-2017 |
| ASTER_DEM | GRID | ≅1 | - | Topography Map (Elevation/Slope) |
| Population Density | GRID | ≅1 | 2015 | Human population per unit area |
| MODIS_ MCD12Q1 | GRID | ≅ 0.25 | 2017 | Land Cover |
| Location of Petroleum Fields | Vector (.shp) | - | - | Distance from Petroleum Fields |
| Location of Faults | Vector (.shp) | - | - | Distance from Faults |
| Location of Major Rivers | Vector (.shp) | - | - | Distance from Rivers |

**Table 2: GLDAS products used to remove the hydrological effects from GRACE observations (Source: https://giovanni.gsfc.nasa.gov/giovanni/)**

| Product Name | Unit | Temporal Resolution | Spatial Resolution | Used Time Period |
|---|---|---|---|---|
| Soil Moisture Content (From 0 to 200 cm depth) GLDAS_NOAH10_M v2.1 | $Kg/m^2$ | Monthly | ≅111 $Km^2$ | 2002/04/18 to 2017/01/21 |
| Snow Water Equivalent GLDAS_NOAH10_M v2.1 | $Kg/m^2$ | Monthly | ≅111 $Km^2$ | 2002/04/18 to 2017/01/21 |
| Storm Surface Runoff GLDAS_NOAH10_M v2.1 | $Kg/m^2$ | Monthly | ≅111 $Km^2$ | 2002/04/18 to 2017/01/21 |
| Plant Canopy Surface Water GLDAS_NOAH10_M v2.1 | $Kg/m^2$ | Monthly | ≅111 $Km^2$ | 2002/04/18 to 2017/01/21 |

## 3. Results

Figure 3.a illustrates the zoning maps for subsidence obtained using FAHP. The map is classified into five classes, with degrees of fuzzy membership for each pixel ranging between 0 and 1. A value of 0 depicts pixels least susceptible to subsidence (none of the constraints are met), while 1 shows the maximum potential for subsidence (all constraints are met).

Figure 3.b depicts zoning maps obtained using the Boolean method, where, a value of 1 indicates zones that met all the conditions and are highly susceptible to subsidence. Both obtained maps were finally rescaled and combined to form a more reliable map. For the rescaling, zones in the FAHP with degrees of fuzzy memberships greater than 0.7 were given a value of 1 and those with lower degrees of membership were mapped to 0. The new AHP map was than scaled along with the Boolean map and both maps were finally intersected to obtain the final binary zoning map of subsidence for the Tigris and Euphrates Basin (TEB) (figure 4). As shown in figure 4, red regions the areas highly susceptible to subsidence, while those with a low or zero susceptibility are shown in green. According to figures 3.a, 3.b, and 4, out of the total area of the study region, approximately 2.62%, 3.54%, and 1.39% of the areas were highly susceptible to subsidence, respectively (table 3). The final map (figure 4) was then divided, based on pixel density, into 8 zones for further analysis. It can be seen that the highly susceptible zones fall within the political regions of Iraq (figure 5).

Table 4 and figure 6 show the analytical results as well as the cause-effect relationships between the effective parameters obtained using DEMATEL method. According to D+R and D-R values, each depicting the significance and the impressibility and effectiveness of the parameters, respectively, elevation and distance from rivers seem to be the most effective parameters, respectively, while land cover, TWUC, and population are the most impressible parameters compared to the others.

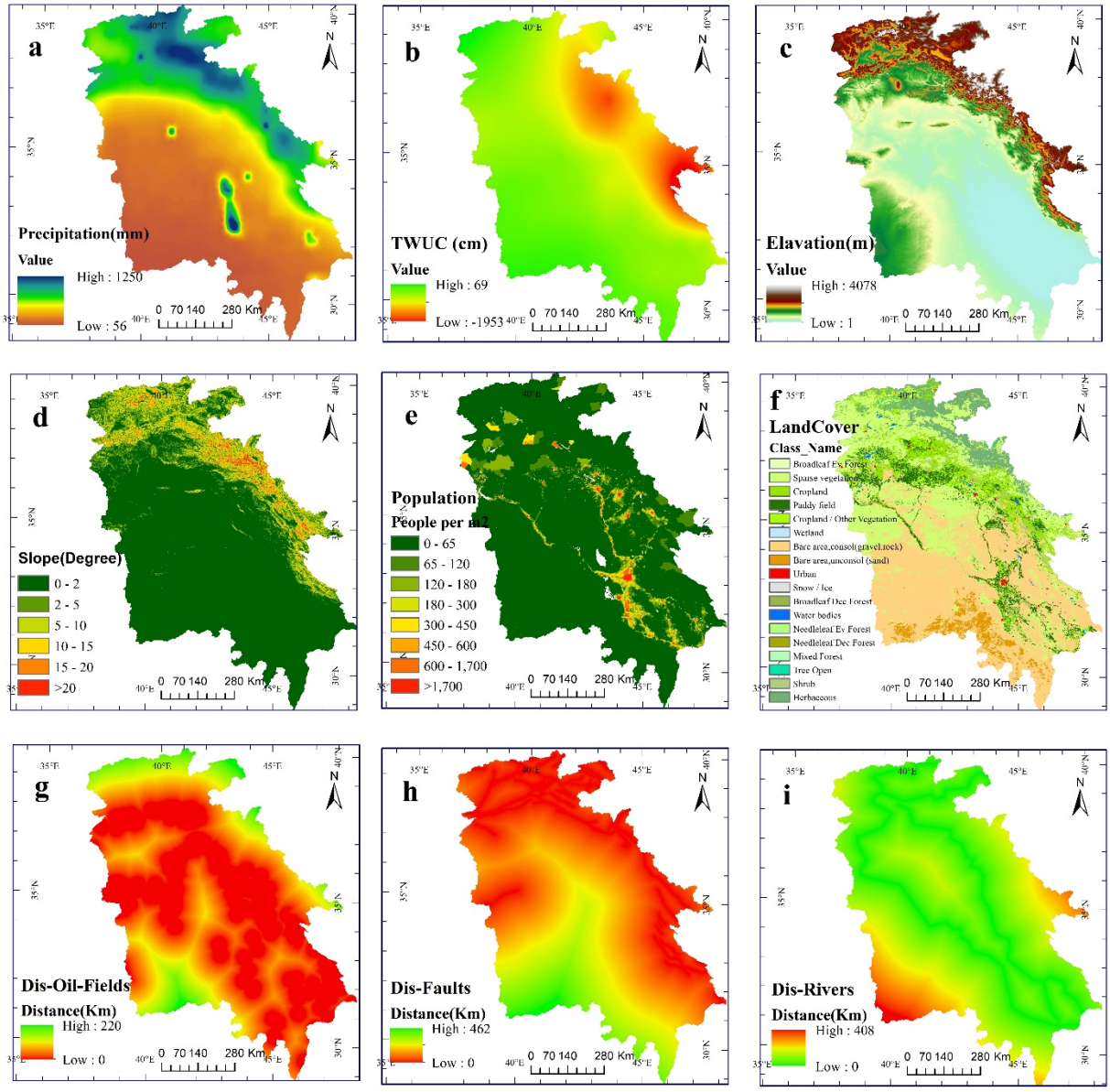


**Figure 2. Map prepared for each effective factors on subsidence: a (Average Annual Cumulative Precipitation 1998-2018), b (Total Water Underground Changes 2002-2017), c (Elevation), d (Slope), e (Human Population Density), f (Land Cover), g (Distance from Petroleum Fields), h (Distance from Faults), i (Distance from Rivers).**

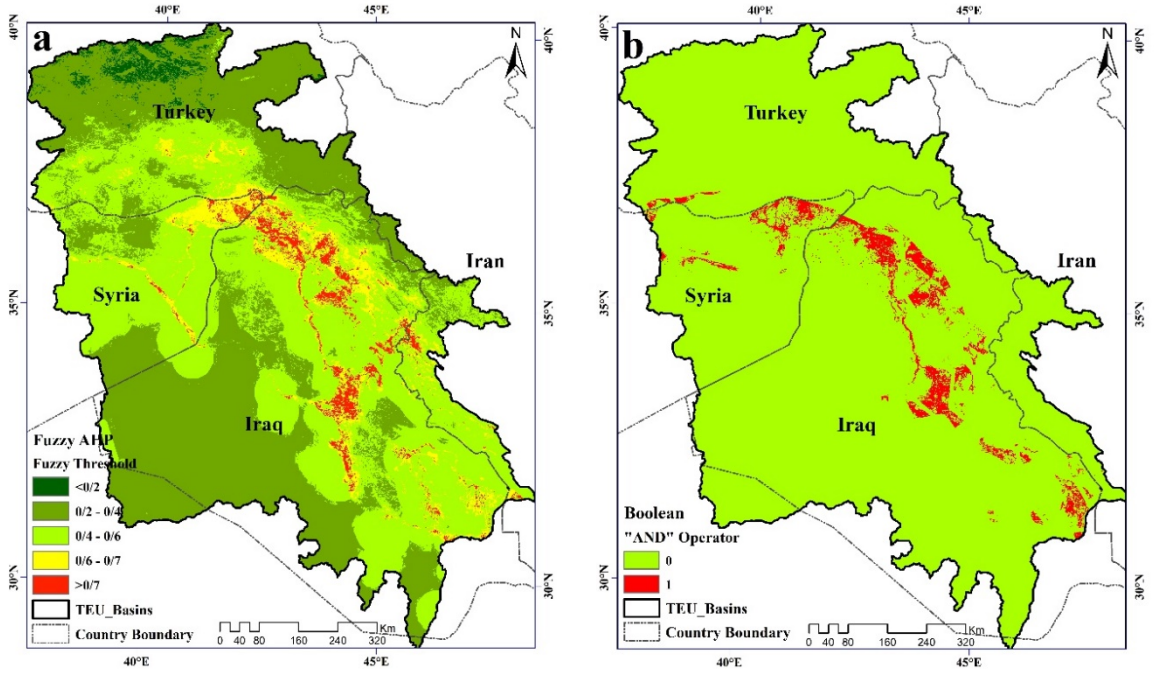


**Figure 3. a (FAHP Method _De-Fuzzy Map of Susceptibility to land subsidence Classes), b (Boolean Method_ "AND" operator_ Susceptibility to land subsidence Classes).**

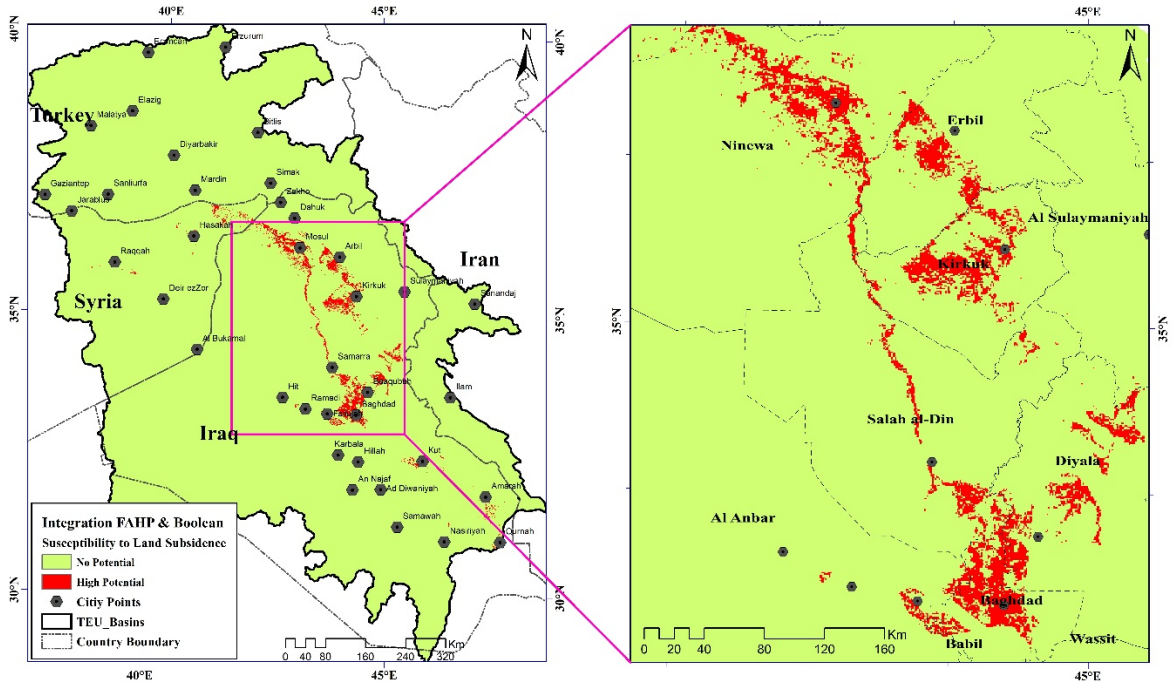


**Figure 4. Integration of FAHP-Boolean Method_ High Susceptibility to land subsidence.**

**Table 3: The results of land subsidence susceptibility zoning in TEB.**

| Objective | Model | Number of Pixels | Area ($Km^2$) | Percentage |
|---|---|---|---|---|
| High Susceptibility to Land Subsidence | FAHP | 23929 | 23929 | 2.62 |
| | Boolean | 32405 | 32405 | 3.54 |
| | FAHP-Boolean | 12756 | 12756 | 1.39 |

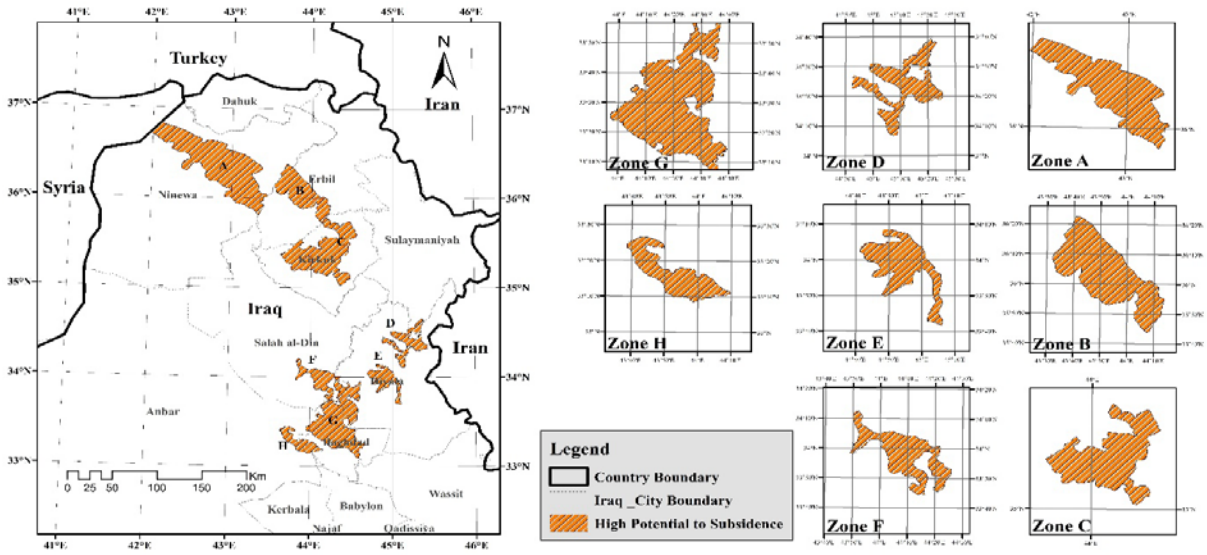


**Figure 5. Zones with High Potential to Land Subsidence**

**Table 4: The results of DEMATEL method - Analysis of the relationship between parameters affecting land subsidence. D+R (Prominence) and D-R (Relation)**

| | Dis Oil | Dis Fault | Precipitation | TWUC | Elevation | Slope | Dis River | Land cover | Population |
|---|---|---|---|---|---|---|---|---|---|
| **D+R** | 0/54 | 0/31 | 1/55 | 2/79 | 1/73 | 1/03 | 1/45 | 3/07 | 2/83 |
| **D-R** | 0/26 | 0/03 | 0/57 | -1/33 | 1/45 | 0/52 | 1/17 | -1/45 | -1/24 |

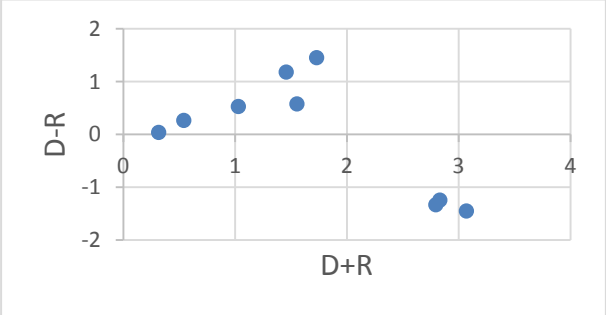


**Figure 6. D+R (Prominence) and D-R (Relation)**

## 4. Discussion and Conclusion

As observed from figure 5, all eight zones are located within the class of high susceptibility to subsidence, with all nine parameters reaching their thresholds (indicating subsidence). Population density in the selected zones is higher compared to other areas and are comprised primarily of agricultural and paddy fields. This is further verified by looking at land cover and population density maps for the region. The remaining regions of the TEB have lower populations with scattered vegetation, shrubs, and bare soil as the dominant land cover. The bulk of the selected zones (with the exception of Zone H located on the Euphrates river route) are placed on fertile plains alongside the Tigris river, which is home to the majority of Iraqi population.

As a general rule, population always affects land-use. Land-use and land cover on the other hand are directly related to water supply and use. Although the southern regions of the basin, mainly comprised of bare soil and scattered vegetation and low in population, savor the least amount of precipitation, the patterns of change from 2002-2017 indicate a positive correlation between these regions and groundwater status. On the other hand, the selected zones, albeit close to both the Tigris and Euphrates rivers and with higher rates of precipitation, have a negative correlation with changes in groundwater. This is most probably due to the expanding population of the mapped zones as well as the corresponding land use and water usage in such regions. The mapped zones are mainly comprised of lowlands and flat plains with a low rate of precipitation relative to northern parts of the basin. Almost all of the selected regions are located on the gas and oil fields and are highly susceptible to subsidence given the long-term excavations for oil and gas. Results from the DEMATEL analysis showed that land cover, TWUC, and population were the key influential factors with a strong correlation with

other parameters, which also hints at the possibility of implicitly obtaining information from other parameters given these three key factors. This is significantly important in cases where data is limited and knowledge of these three parameters alone can be used to make reliable predictions about the possibility of land subsidence.

## References

[1] D.L. Galloway, K.W. Hudnut, S.E. Ingebritsen, S.P. Philis, G. Peltzer, F. Rogez, and P.A. Rosen, "Detection of aquifer system compaction and land subsidence using interferometric synthetic aperture radar, Antelope valley, Mojave Desert, California," *Water Resour. Res.*, 34, 2573-2585, 1998.

[2] F. Amelung, D.L. Galloway, J.W. Bell, H.A. Zebker, and R.J. Laczniak, "Sensing the ups and downs of Las Vegas: InSAR reveals structural control of land subsidence and aquifer system deformation," Geology, 27, 6, 483-486, 1999.

[3] H.Z. Abidin, R. Djaja, D. Darmawan, S. Hadi, A. Akbar, H. Rajiyowiryono, Y. Sudibyo, L. Meilano, M. A. Kusuma, J. Kahar, and C. Subarya, "Land subsidence of Jakarta (Indonesia) and its geodetic monitoring system," Nat. Hazards, 23, 365-387, 2001.

[4] A. Schmidt, and R. Burgmann, "Time-dependent land uplift and subsidence in the Santa Clara valley, California, from a large interferometric synthetic aperture radar data set," J. Geophys. Res, 108, B9, 2416, 2003.

[5] R. Lanari, P. Lundgren, M. Manzo, and F. Casu, "Satellite radar interferometry time series analysis of surface deformation for Los Angeles, California," Geophys. Res. Lett., 31, L23613, 2004.

[6] M. Motagh, Y. Djamour, T.R. Walter, H.-U. Wetzel, J. Zschau, and S. Arabi, "Land subsidence in Mashhad Valley, northeast Iran: results from InSAR, leveling and GPS," Geophys. J. Int., 168, 518-526, 2007.

[7] D.C. Helm, "One -Dimensional Simulation of Aquifer System Compaction near Pixley," water resources research, 13, 3, 375-391, 1976.

[8] J. Hoffman, S. A. Leake, D. L. Galloway, and A. M. Wilson, "MODFLOW-2000 ground-water model-user guide to the subsidence and aquifer-system compaction (SUB) package," U.S. Geological Survey Open-File Report 03-233, 2003.

[9] S. Lee, and I. Park, "App.lication of decision tree model for the ground subsidence hazard mapp.ing near abandoned underground coal mines," J. of Environmental Management, 127, 166–176, 2013.

[10] S. Swenson, and J. Wahr, "Methods for inferring regional surface mass anomalies from GRACE measurements of time-variable gravity," J. Geophys. Res., 107, B9, 2193, 2002.

[11] S. C. Swenson, and J. Wahr, "Monitoring the water balance of Lake Victoria, East Africa, from space," J. Hydrology, 370(1–4), 163–176, 2009.

[12] M. Cheng, J. C. Ries, and B. D. Tapley, "Variations of the Earth's figure axis from satellite laser ranging and GRACE," J. Geophys. Res.,116, B01409, 2011.

[13] S.C. Swenson, D.P. Chambers, and J. Wahr, "Estimating geocenter variations from a combination of GRACE and ocean model output," J. Geophys. Res.-Solid Earth, Vol. 113, Issue: B8, Article B08410, 2008.

[14] C. Jekeli, "Alternative methods to smooth the Earth's gravity field," Dep. of Geod. Sci. and Surv., Ohio State University, Columbus. Rep. 327, 1981.

[15] G. Joodaki, "Earth Mass Change Tracking Using GRACE Satellite Gravity Data," Ph.D. thesis, Norwegian Univ.